Structure of a CH₃S Monolayer on Au(111) Solved by the Interplay between Molecular Dynamics Calculations and Diffraction Measurements

R. Mazzarello,[1,2] A. Cossaro,[3] A. Verdini,[3] R. Rousseau,[1] L. Casalis,[4] M. F. Danisman,[5] L. Floreano,[3] S. Scandolo,[2] A. Morgante,[3,6] and G. Scoles[1,4,5]

[1]*International School for Advanced Studies, Trieste, Italy*
[2]*The Abdus Salam International Centre for Theoretical Physics and INFM/Democritos National Simulation Center, Trieste, Italy*
[3]*INFM-CNR Laboratorio TASC, Trieste, Italy*
[4]*Sincrotrone Trieste S.C.p.A., Trieste, Italy*
[5]*Department of Chemistry, Princeton University, Princeton, New Jersey, USA*
[6]*Department of Physics, Trieste University, Trieste, Italy*

We have investigated the controversy surrounding the $(\sqrt{3} \times \sqrt{3})R30°$ structure of self-assembled monolayers of methylthiolate on Au(111) by first principles molecular dynamics simulations, energy and angle resolved photoelectron diffraction, and grazing incidence x-ray diffraction. Our simulations find a dynamic equilibrium between bridge site adsorption and a novel structure where 2 CH₃S radicals are bound to an Au adatom that has been lifted from the gold substrate. As a result, the interface is characterized by a large atomic roughness with both adatoms and vacancies. This result is confirmed by extensive photoelectron and grazing incidence x-ray diffraction measurements.

Self-assembled monolayers (SAMs) of thiolates on metal surfaces are ubiquitous in the field of nanoscience with potential applications ranging from molecular electronics [1] to biomembranes [2,3] and nanopatterning [4]. Critical for understanding the growth mechanism [5] and the electrostatic properties [6] of these materials is detailed knowledge of the structure of the molecule-metal interface. Yet, despite significant efforts, this very aspect of the structure of these systems is still debated. Contradictory results are obtained even for the prototypical case of methylthiolate (MT) CH₃S adsorbed on the Au(111) crystal surface. While theoretical simulations have proposed a bridge bonding site for the S atom of MT adsorbed on a flat Au(111) terrace [7,8], the most recent experimental investigations by photoelectron diffraction (PED) [9] and normal incidence x-ray standing waves (NIXSW) [10] suggest a preference for the ontop site. Observations have shown the occurrence of adatoms [5,11], vacancies, and etch pits [4,12] on the metal surface, yet how these features are connected to the interface structure remains unanswered. Simulations have shown that vacancies can enhance the adsorption energy of thiolates [13] and may be necessary in the cleavage of the S-H bond [14]. A recent scanning tunneling microscopy study has suggested the importance of adatoms in film growth and in lifting the Au surface herringbone reconstruction [5]. The presence of these defects introduces new possibilities for resolving the controversy around the interface structure, but also new difficulties because of the increased number of degrees of freedom.

Given the hypothesis of a restructuring of the Au-thiolate interface, we decided to employ density functional theory (DFT)-based molecular dynamics (MD) calcula-tions to determine a realistic structural model, from which to fit our experimental data obtained using PED and grazing incidence x-ray diffraction (GXRD). The choice of the single carbon MT allows us to evaluate local structures without loss of accuracy due to the inability of DFT to describe the van der Waals interactions that partially stabilize longer chain systems. The small hydrocarbon chain also allows for an unhindered detection of S atom photoelectrons, backward scattered from the Au substrate. Finally, GXRD can effectively probe the Au surface reconstructions. In a final step, we reexamine our experimental models with additional simulations for further validation of our conclusions.

Samples were prepared in ultrahigh vacuum conditions at the ALOISA beam line, where both photoemission spectroscopy, x-ray photoelectron spectroscopy, and surface GXRD can be performed *in situ* [15]. The Au(111) substrate was cleaned by standard sputtering and annealing procedures. Dosing dimethyl disulfide at room temperature yields the formation of the $(\sqrt{3} \times \sqrt{3})$-$R30°$ MT phase [16,17], corresponding to the saturation of the first molecular layer. The sample was cooled to ~170 K before illumination by synchrotron radiation in order to minimize radiation damage due to secondary electron emission [18]. We measured S 2*p* core level spectra in order to detect the structural information carried by the photoelectrons backward scattered by the underlying Au atoms. We collected both angular-dependent PED, at a fixed photon energy of 250 eV, and energy-dependent PED in normal emission. PED polar scans were measured by collecting the photoemission signal as a function of the emission angle θ and rotating the electron analyzer in the scattering plane for different sample azimuthal orientations. The photon en-

ergy range scanned for energy-dependent PED was 250–630 eV. The data points shown in Fig. 1 represent the PED anisotropy $\chi = (I - I_0)/I_0$, where I is the integrated intensity of the S $2p_{3/2}$ component; I_0 is a smoothly varying background of I, evaluated by a low order polynomial fitting. PED data have been simulated with the MSCD program [19]. X-ray diffraction measurements have been performed at 7000 eV photon energy and 0.5° grazing angle. Out-of-plane measurements (rod scans) were performed for nine inequivalent diffraction peaks (including truncation and surface reconstruction rods), in addition to a reflectivity scan. GXRD data were simulated with the ROD program [20].

DFT calculations were performed using a gradient corrected functional [21], norm-conserving pseudopotentials, and a plane wave basis set with an energy cutoff of 45 Ry. Car-Parrinello MD simulations [22] were conducted, using the CPMD code [23], to generate 10 ps trajectories after ≈ 4 ps of equilibration; Nosé-Hoover thermostat chains on both electrons and nuclei are employed to enforce adiabaticity; see Ref. [24] for an evaluation. All reported trajectories were performed in a 2×2 supercell of the $(\sqrt{3} \times \sqrt{3})R30°$ structure, modeled as a 4 Au atom layer

slab with a 10 Å vacuum layer, and the Γ point for Brillouin zone sampling. Adsorption energies are calculated in a grand-canonical definition $E_{ad} = E[Au(111)] + E(MT) - E(MT/Au) - N^*E(Au\ bulk)$, where $E(MT/Au)$, $E[Au(111)]$, and $E(MT)$ are the energies of the MT/Au, Au(111) surface slab, and gas phase MT, respectively, and N is the number of bulk Au atoms, with energy $E(Au\ bulk)$, required to account for vacancies and/or adatoms. E_{ad} are calculated using 6 Au atom layer slabs, the Mermin functional with electronic temperature of 200 K, and up to $8 \times 8 \times 1$ Monkhorst-Pack k-point meshes.

To generate new structural models, we employ our MD simulations to explore the available configuration space in an unbiased way. We first consider our results at 300 K starting from MT molecules at ontop sites, which is a local minimum ($E_{ad} = 1.42$ eV) higher in energy than the bridge site ($E_{ad} = 1.72$ eV). This site is short-lived ($t < 4$ ps), indicating a small energy barrier for the MT to migrate to either bridges or a novel motif, where a single Au atom is pulled out of the surface, by ≈ 2.0 Å, and shared by two MTs. This feature, denoted MT-Au-MT, remains stable for the entire 10 ps trajectory. The structure quenched from the last MD configuration consists of two bridges and one MT-Au-MT and has $E_{ad} = 1.80$ eV; see Fig. 2. This small energy preference, with respect to the
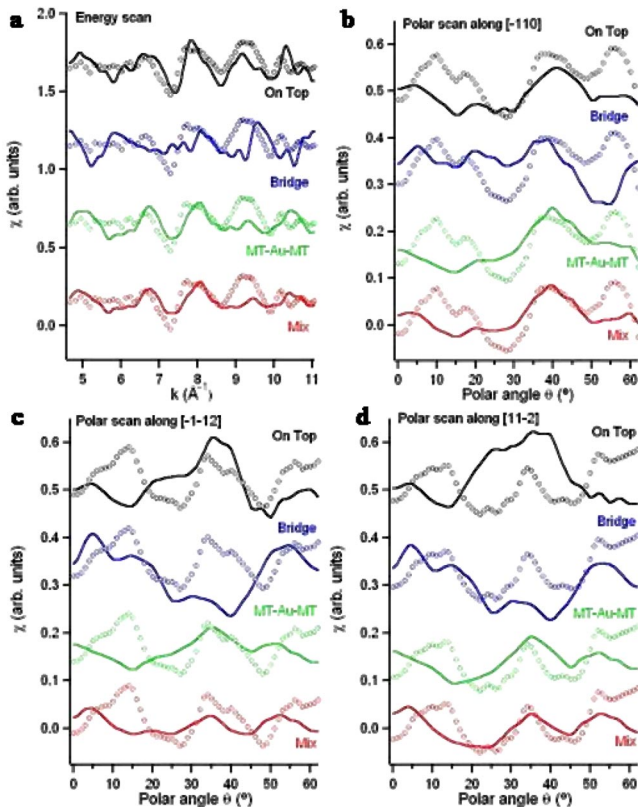

FIG. 1 (color online).   PED fits (a)–(d): exp, (circles); fit (lines): ontop (black), bridge (blue), MT-Au-MT (green), disordered model (red). (a) Energy resolved spectrum taken in normal emission at a grazing angle of 4°. (b)–(d) Selected angle resolved PED polar scans along (b) $[-110]$, (c) $[-1-12]$, and (d) $[11-2]$ directions.

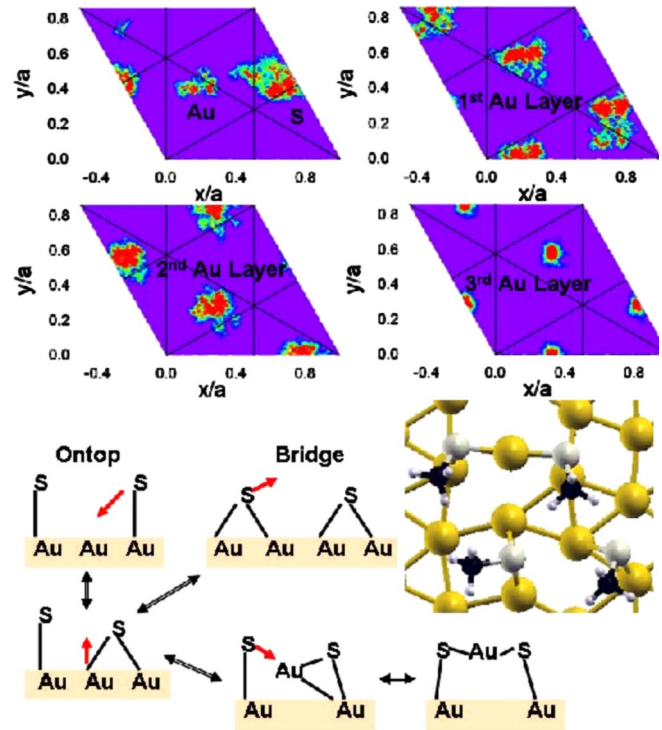
FIG. 2 (color online).   (Upper panels) Position density distribution $P(x, y)$ in the $(\sqrt{3} \times \sqrt{3})R30°$ unit cell, obtained from 300 K MD. The superimposed hexagonal lattice corresponds to the positions of 1st layer gold atoms of Au(111). (Lower panel) Schematic representation of equilibrium between MT at bridge and MT-Au-MT. (Inset) Structure of 1st Au layer and adsorbates obtained by quenching the 600 K MD simulations.

bridge site, can be traced to the MT-Au-MT unit as shown by $E_{ad} = 1.83$ eV for a structure consisting only of this feature. Simulations at 300 K starting from the bridge configuration do not exhibit this transformation; however, raising the temperature to 600 K sees the formation of an MT-Au-MT within 2 ps. This indicates that the bridge $\rightarrow$ MT-Au-MT transformation has an appreciable energy barrier but is still feasible at low temperatures on longer time scales than our simulations. Upon quenching, this latter simulation also yields a MT-Au-MT and two bridging MTs. In total, our observations suggest that both bridge and MT-Au-MT configurations exist in a dynamic equilibrium; see Fig. 2.

The formation of MT-Au-MT units is not consistent with the $(\sqrt{3} \times \sqrt{3})R30°$ cell. This symmetry can be recovered by noting that MT-Au-MT/bridge interconversion is feasible, though slow on the picosecond time scale, and would result in a disordering of the MT over multiple sites; note that our short simulation times do not allow us to address if the disorder is static or dynamic. To elucidate how this equilibrium can manifest itself in an average structure, we compile position density maps $P(x, y)$ in a $(\sqrt{3} \times \sqrt{3})R30°$ unit cell for Au and S, using our 300 K trajectory (see Fig. 2). The S atom in the topmost layer displays a broad density basin because it is spread out over both bridge and MT-Au-MT sites. The Au adatom lies directly on the ideal line between 2 S atoms and has a coverage of ≈ 0.08 monolayers (ML). $P(x, y)$ for the first Au layer displays broad, over 1 Å, *bimodal* distributions for each atom, resulting from the different positions that they occupy depending on the binding configuration of the nearby MT. This Au layer has a net vacancy coverage of 0.08 ML owing to the promotion of the adatoms into the MT-Au-MT structure. The 2nd and 3rd layers of Au atoms display *unimodal* distributions in $P(x, y)$ which are broad in the 2nd and bulklike in the 3rd, indicating that the disorder rapidly decays away from the surface.

We performed extensive PED measurements to compare with our theoretical model structure. We verified that our experimental energy scan PEDs are in good agreement with those of Ref. [9] and also that the energy resolved PED anisotropy is well reproduced [see Fig. 1(a)] by an ontop structure, with reliability factor $r_f = 0.49$. This can be improved by adjusting the S-Au bond length to 2.49 Å and the tilt angle with respect to the surface normal to $\Theta_{AuS} = 10°$, to form a "quasi-ontop" structure, $r_f = 0.44$. This model is not consistent with the angle resolved PED data; see Figs. 1(b)–1(d), where our best fit yields $r_f = 0.81$ using data from all polar scans. Likewise, a model where the thiols sit directly on top of an adatom [11] provides good fits to the energy resolved data $r_f = 0.43$ but is a poor match to the angle resolved PED, $r_f = 0.78$. Better agreement is obtained by considering a mixed MT-Au-MT/bridge model. In this case, the PED scattering is calculated as the sum of intensities from both configurations, employing our theoretical atom positions without

adjusting any structural parameter, and varying only the relative site occupation. By minimizing r_f for both energy and angle resolved data separately, we obtained a MT-Au-MT:bridge occupancy ratio of about 3:1, corresponding to an adatom coverage of about 0.25 ML. Uncertainty in this ratio is large, since a 1:1 occupation (that observed in the MD simulations) exhibits only modest increases, 0.07, in r_f. Our model provides a best fit of the energy scan PED ($r_f = 0.52$) which is comparable with that of the ontop model, but the fit to the angle resolved PED is significantly improved, $r_f = 0.48$; see Figs. 1(b)–1(d). The PED simulations are not sensitive to the number and location of vacancies, as structures of both bridging MT and MT-Au-MT with or without vacancies have similar angle resolved distributions (and r_f); however, they are sensitive to the presence of adatoms, as the quasi-ontop model and MT-Au-MT species have very different angle resolved r_f (0.8 and 0.5, respectively), despite their similar S positions. Finally, as the average S position for our model is located almost at the ontop position, it should also account for the recent NIXSW data [10].

Further evidence in favor of our model is provided by GXRD measurements. Noting that these measurements are almost unaffected by the S atoms (due to the large difference of the atomic form factor of Au and S), the pronounced intensity drop (as compared to the perfect surface) observed in the x-ray reflectivity at large perpendicular momentum transfer L indicates an increase of roughness in the surface (see Fig. 3). The whole set of rod scans is shown in Fig. 4 together with best fit simulations. The reflectivity data alone can be accounted for by a bulklike surface with additional roughness, as found for a film in the presence of vacancy islands, but this model cannot provide even qualitatively correct fits to the (2, 0) and (0, 2) rod scans. We attribute the observed surface roughness to a distribution of vacancies and adatoms disordered over multiple sites due to dynamical fluctuations, as suggested by our MD simulations. We made use of a model with a double Au population in the surface layer (with atomic occupancy lower than 0.5) to mimic a distri-
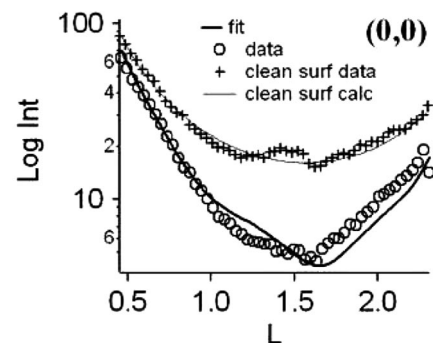

FIG. 3. Measured x-ray reflectivity (arbitrary units) as a function of perpendicular momentum transfer L in units of $2\pi/c$, where $c = 7.06$ Å is 3 times the (111) bulk plane spacing.
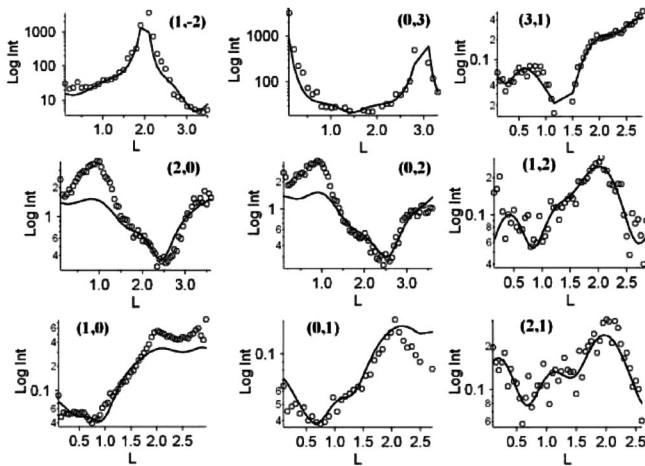
FIG. 4. Measured diffraction intensity (arbitrary units) as a function of perpendicular momentum transfer L (see Fig. 3 for definition); circles, experimental data; solid line, best fit; (h, k) indexes refer to the $(\sqrt{3} \times \sqrt{3})R30°$ unit cell.

bution of atoms disordered over multiple sites. Within this model, the possible occurrence of vacancies and adatoms in multiple sites can be described by variation in the fractional occupancy of each site. In the GXRD simulations, we also varied S atom positions, starting near ontop sites, but, due to the relatively small scattering intensity of S, the reliability of this determination is low. Thus, in the final fits we kept the S at the quasi-ontop site position, as derived from the PED analysis. We obtained an Au adatom coverage of 0.1 ML, at sites located between nearest neighbor S atoms, similar to the theoretical $P(x, y)$; see Fig. 2. After summation of the fractional occupancies of each atom in the surface layer, we found a 0.2 ML population for vacancies. Significant displacements of the second Au layer atoms are also present, as expected by the large concentration of vacancies [25].

The structure resulting from GXRD fits contains more vacancies than accounted for in our MD simulations. Hence, as a further cross-check on our conclusions, we employed the experimental positions and occupancies as a starting point for further simulation. By employing finite temperature MD followed by quenching, we relaxed a supercell of 9 MTs with 3 adatoms and 6 vacancies which resulted in a structure with 3 MT-Au-MT and 3 bridges, with an $E_{ab} = 1.92$ eV—i.e., stronger adsorbate binding than obtained above. Thus, the experimental structure fits well with our interpretation of the interface as consisting of an equilibrium distribution of sites with the caveat that additional vacancies further lower the energy [13,14].

We have presented a novel approach on how to arrive at a model that explains the structural measurements of MT/Au(111) SAMs. Our model resolves the theory-experiment discrepancy that has been prominent in the literature. As a likely consequence of our proposed disordered model, we note that the well-known formation of

superlattices [26–28] may be a result of an ordering among binding sites and vacancies. In general, our results underscore the importance of disorder at molecule-metal interfaces. The flat potential energy landscape observed here should be ubiquitous for these junctions, which in turn implies that a single well-defined binding geometry may not necessarily be an appropriate description. Special care must be given to examining these "problematic systems" by deploying multiple experimental or theoretical techniques which probe different aspects of the structure on different time scales.

[1] F. Schreiber, Prog. Surf. Sci. **65**, 151 (2000).
[2] K. Uvdal and T. P. Vikinge, Langmuir **17**, 2008 (2001).
[3] A. Cossaro *et al.*, Langmuir **22**, 11 193 (2006).
[4] G. Yang and G.-Y. Liu, J. Phys. Chem. B **107**, 8746 (2003).
[5] P. Maksymovych *et al.*, Phys. Rev. Lett. **97**, 146103 (2006).
[6] V. De Renzi *et al.*, Phys. Rev. Lett. **95**, 046804 (2005).
[7] M. C. Vargas *et al.*, J. Phys. Chem. **105**, 9509 (2001).
[8] T. Hayashi *et al.*, J. Chem. Phys. **114**, 7615 (2001).
[9] H. Kondoh *et al.*, Phys. Rev. Lett. **90**, 066102 (2003).
[10] M. G. Roper *et al.*, Chem. Phys. Lett. **389**, 87 (2004).
[11] M. Yu *et al.*, Phys. Rev. Lett. **97**, 166102 (2006).
[12] G. E. Poirier, Chem. Rev. **97**, 1117 (1997).
[13] L. M. Molina and B. Hammer, Chem. Phys. Lett. **360**, 264 (2002).
[14] J. G. Zhou and F. Hagelberg, Phys. Rev. Lett. **97**, 045505 (2006).
[15] L. Floreano *et al.*, Rev. Sci. Instrum. **70**, 3855 (1999).
[16] R. G. Nuzzo *et al.*, J. Am. Chem. Soc. **109**, 733 (1987).
[17] J. Noh and M. Hara, Langmuir **16**, 2045 (2000).
[18] P. Feulner *et al.*, Surf. Sci. **593**, 252 (2005).
[19] MSCD Version 1.37, Y. Chen and M. A. Van Hove; see www.sitp.lbl.gov/index.php?content=/mscdpack.
[20] E. Vlieg, J. Appl. Crystallogr. **33**, 401 (2000).
[21] J. P. Perdew *et al.*, Phys. Rev. Lett. **77**, 3865 (1996).
[22] R. Car and M. Parrinello, Phys. Rev. Lett. **55**, 2471 (1985).
[23] CPMD V3.9 Copyright IBM Corp. 1990–2001, Copyright MPI für Festkoerperforschung Stuttgart 1997–2001.
[24] R. Rousseau, R. Mazzarello, and S. Scandolo, Chem. Phys. Chem. **6**, 1756 (2005).
[25] Cell axes: $a = b = 4.99$ Å, $\gamma = 60°$; 1st and 2nd layer atomic positions (x, y, z, occupancy): Au1(0.48, −0.47, 14.48, 0.57), Au2(−1.44, −1.52, 14.00, 0.35), Au3(2.77, 0.59, 14.57, 0.35), Au4(2.55, −1.87, 14.17, 0.43), Au5(0.65, 2.08, 14.26, 0.46), Au6(0.77, 1.08, 13.77, 0.2), Au$_{ad}$(0.13, 2.09, 16.13, 0.3), S(−0.12, −0.12, 16.41, 1.0), Au1$_{2L}$(1.48, 0.90, 11.81, 1.0), Au2$_{2L}$(2.93, −1.59, 12.13, 1.0), Au3$_{2L}$(0.02, 3.37, 11.85, 1.0).
[26] L. H. Dubois, J. Chem. Phys. **98**, 678 (1993).
[27] M. F. Danisman *et al.*, J. Phys. Chem. **106**, 11 771 (2002).
[28] V. De Renzi *et al.*, J. Phys. Chem. B **108**, 16 (2004).